Comparison of Inverter Controllers with Synthetic Inertia and Harmonic Compensation Features

Thiago Silva Amorim, Daniel Carletti, Lucas Frizera Encarnação

***Abstract*—This paper proposes a comparison of three strategies that combine the features of a virtual synchronous generator (VSG) and an active filter on a three-phase three-leg inverter. The VSG controller determines the current reference at the fundamental component, which provides synthetic inertia to the inverter that contributes to the system stability, and the active filter controller calculates the reference harmonic currents to mitigate the harmonic currents in a power system. The three control strategies are simulated using a real-time test-bench in two scenarios where the power system voltage has different harmonic voltage content and the simulation results were presented to compare the three inverter controllers' performance in the two proposed scenarios. The VSG control is compared to a constant active and reactive power control and the VSG contribution to the system stability is discussed.**

***Keywords*: active filter, harmonic compensation, power quality, synthetic inertia, virtual synchronous generator.**

I. Introduction

SINCE the 1990s, due to the development of new technologies and regulatory changes, there is an increasing interest in distributed generation (DG) units, which are small-scale generation units distributed in the power system. Some DG sources are connected to the power system through a DC-AC interface equipment, such as static converters. That interface equipment usually does not have rotational inertia and, unlike synchronous machines, does not naturally contribute to the system stability [1].

The virtual synchronous generator (VSG) is an alternative to stabilize power systems with a large presence of non-inertial sources. The VSG control provides to the inverter synthetic inertia through the virtualization of a synchronous generator dynamic behavior [2]. This feature allows converters to contribute to the electrical systems stability and not compromise the system operation in the event of disturbances. The stability of the power system can be classified according to the time frame and which system variable is being disturbed. Thus, the power systems stability study includes the voltage, frequency, and rotor angle stability [3]. The VSG contribution to frequency and rotor angle stability, transient and small-signal stability, in this case, is widely discussed in the literature [4].

In addition to the problems related to the electrical system stability, the significant increase of nonlinear loads is another concern in the distribution systems [5][6]. Nonlinear loads change the sinusoidal nature of the AC currents and, consequently, of the AC grid voltages. The harmonic current flow decreases the system power quality and it can increase losses and heat in various electromagnetic devices [7][8]. The application of active filters can decrease the presence of harmonics in an electrical system [5]. Active filter controllers need to measure voltages and/or currents to calculate the harmonic reference current to mitigate the harmonic currents from a specific feeder or load or to damp harmonics throughout power distribution systems.

As both VSG and active filter controllers are applied on inverters, some applications combine VSG and harmonic compensation controls. In [9], the harmonic detection controllers measure the voltages at the point of common coupling (PCC) and the load currents to compensate the harmonic currents from a specific load. In [10], the authors use a controller that measures the voltages at the PCC and the feeder current to mitigate selected harmonics from a specific feeder. In [11], the controller is based on voltage detection and measures only the voltage at the PCC to calculate the compensating harmonic current to damp harmonic propagation. However, the use of active filter controllers that need to measure currents to calculate a harmonic current reference can be impracticable in a grid with DG due to the bidirectional power flow. The addition of DG units and grid topology reconfiguration can reverse the power flow at the DG installation point. The line currents can flow to either a feeder bus or a load bus and the control strategies based on the exclusive measurements of load or source currents would not work well. Although the strategy based on only voltage detection is not affected by the bidirectional power flow, voltage harmonics present in the electrical system generators and substations can reduce the effectiveness of harmonic damping. While the strategies presented in [9] and [10] are more suitable for end-users, the strategy used in [11] is more adequate to solve problems of electric power utilities [5].

Despite the proposed work is applied in a low power inverter, both VSG and active filter controller can be used in high power applications [12]-[15]. Thus, the use of a high power inverter with a control combining the VSG and the active filter may be feasible.

In this paper, three control strategies that combine VSG and

This work was supported in part by the Fundação de Amparo à Pesquisa e Inovação do Espírito Santo (FAPES) under Grants 536/2018 and 117/2019 and FAPES / Coordenação de Aperfeiçoamento de Pessoal de Nível Superior (FAPES / CAPES) under Grant 67/2017. This work was supported by the "10 for 10 Typhoon HIL Awards Program".

T. S. Amorim is with Federal University of Espírito Santo, Vitória, ES 29075910 Brazil (e-mail of corresponding author: t.s.amorim@hotmail.com).
D. Carletti is with Federal University of Espírito Santo, Vitória, ES 29075910 Brazil (e-mail: danielc.ufes@gmail.com).
L. F. Encarnação is with Federal University of Espírito Santo, Vitória, ES 29075910 Brazil (e-mail: lucas.encarnacao@ufes.br).

Paper submitted to the International Conference on Power Systems Transients (IPST2021) in Belo Horizonte, Brazil June 6-10, 2021.

active filter features are compared and the performances are discussed. In scenario 1, the power system voltage does not have any harmonic component. In scenario 2, a 0.05 pu fifth harmonic voltage was added to the power system voltage to evaluate the control strategies' performances under distorted grid voltages. The structure of this paper is as follows. Section II shows the modeling equations of an electromechanical synchronous machine (SM) used to calculate the fundamental component of the reference current. Section III presents the three active filter controllers used to detect harmonic currents or voltages. Section IV presents the real-time simulations results of the VSG presented in Section II combined with the three active filter controllers presented in Section III in two harmonic voltage content scenarios. In Section IV, the VSG control is compared to a constant active and reactive power control the VSG control contribution to the system frequency stability. In Section V, the results shown in Section IV are analyzed and discussed.

II. Virtual Synchronous Generator

Through the use of a controller based on the modeling equations of an electromechanical SM, it is possible to control an inverter so that it mimics the behavior of the SM. The inverter operation has an effective inertial characteristic to the system stability. Furthermore, due to the virtualization of the SM model, the VSG is not restricted to physical parameters as SM, such as reactances, inertia, and damping coefficient, making it possible to propose new VSG applications with their parameters being varied in an adaptive way to improve the system stability.

Other authors in the literature have a similar approach. An extended review of existing literature on different VSG implementations can be found in [16]-[18].

The VSG model used in this paper is based on [19]. This model reproduces the stator windings and the mechanical subsystem. Fig. 1 shows a configuration of a VSG connected to a power system.

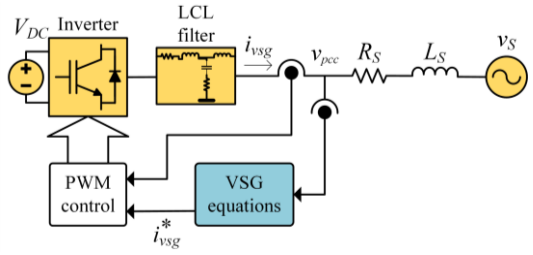

Fig. 1. The basic configuration of a VSG

The stator circuit is described by (1).

$$\vec{e}-\vec{v}_{pcc}=R_{vsg}\vec{i}_{vsg}+L_{vsg}\frac{d\vec{i}_{vsg}}{dt} \quad (1)$$

where $\vec{e}=[e_1 \quad e_2 \quad e_3]^T$ is the induced electromotive force (EMF) at the stator windings, $\vec{v}_{pcc}=[u_1 \quad u_2 \quad u_3]^T$ is the voltage at the PCC, $\vec{i}_{vsg}=[i_1 \quad i_2 \quad i_3]^T$ is the VSG current reference, R_{vsg} and L_{vsg} are the stator virtual resistance and inductance, respectively. The stator inductance L_{vsg} is the series association of LCL filter inductors L_1 and L_f.

$$L_{vsg}=L_1+L_f \quad (2)$$

The current reference can be calculated in the Laplace domain, as in (3).

$$\vec{i}^*_{vsg}(s)=\frac{\vec{e}(s)-\vec{v}_{pcc}(s)}{R_{vsg}+L_{vsg}s} \quad (3)$$

Equations (4) and (5) describe the rotor electromechanical dynamic.

$$T_m-T_e-k_d\Delta\omega=\frac{P_m}{\omega}-\frac{P_e}{\omega}-k_d\Delta\omega=J\frac{d\omega}{dt} \quad (4)$$

$$\frac{d\theta}{dt}=\omega \quad (5)$$

where T_m is the mechanical torque, T_e is the electrical torque, P_m is the mechanical power, P_e is the electrical power, J is the moment of inertia, k_d is the damping factor, ω is the angular velocity, $\Delta\omega$ is the angular velocity deviation, and θ is the rotor angle.

Equations (6) and (7) describe the speed governor and electromagnetic torque T_e equations, respectively.

$$T_m=P_m/\omega_0=(P^*+D_p(\omega_0-\omega))/\omega_0 \quad (6)$$

$$T_e=P_e/\omega_0=(u_1i_1+u_2i_2+u_3i_3)/\omega_0 \quad (7)$$

where P^* is the active power reference, D_p is the droop coefficient and ω_0 is the reference angular velocity.

If the VSG controller should be able to regulate v_{pcc}, the adjustable induced EMF amplitude is given by (8).

$$E_p=E_0+(V_0-V)K_u/s \quad (8)$$

where E_0 is the induced EFM reference, V_0 is the reference peak voltage, V is the peak VSG output voltage and K_u is the voltage controller gain.

If the VSG controller should control the VSG reactive power output (Q) instead of regulating v_{pcc}, the adjustable induced EMF amplitude is given by (9).

$$E_p=E_0+(Q_0-Q)(K_{pQvsg}+K_{iQvsg}/s) \quad (9)$$

where Q_0 is the active power reference, K_{pQvsg} is the controller proportional gain and K_{iQvsg} is the controller integral gain.

The VSG induced EMF in abc frame is shown in (10).

$$\vec{e}=\begin{pmatrix}e_1\\e_2\\e_3\end{pmatrix}=E_p\begin{pmatrix}sin(\theta)\\sin(\theta-2\pi/3)\\sin(\theta+2\pi/3)\end{pmatrix} \quad (10)$$

With the addition of mechanical equations (4) and (5) in the active power control, the inverter can respond to frequency disturbances like a synchronous machine. With a frequency variation in the system, the VSG control injects active power to compensate for the momentary disturbance [16].

III. Harmonic Detection

Three active filter control strategies were used in this work. Fig. 2 shows an active filter connected to a power system and the measurements required to implement the harmonic detection controllers.

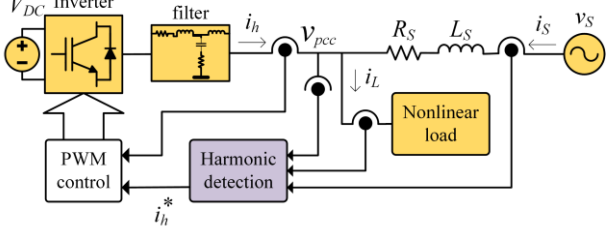

Fig. 2. The basic configuration of a shunt active power filter

Control Strategy 1 (C1) measures the load current $i_{L(abc)}$ and the voltage at the PCC to compensate harmonic currents from a specific load. Control Strategy 2 (C2) measures the source currents $i_{S(abc)}$ and the voltage at the PCC to mitigate the harmonic currents from a specific feeder. Control Strategy 3 (C3) measures only the voltage at the PCC and is an approach based on harmonic voltage detection. All strategies used in this work are based on the instantaneous active and reactive power theory (*pq* Theory) [5]. The Clarke transformation maps measured instantaneous voltages and currents in the *abc*-axes into instantaneous voltages and currents on the *αβ0*-axes. The load current $i_{L(abc)}$ is only measured in C1 and source current $i_{S(abc)}$ is only measured in C2.

In C1, a Dual Second Order Generalized Integrator - Frequency Locked Loop (DSOGI-FLL) [20] is used to extract the fundamental component positive-sequence $v'_{(\alpha\beta0)}$ of $v_{pcc(\alpha\beta0)}$. The load current $i_{L(\alpha\beta0)}$ and $v'_{(\alpha\beta0)}$ are used in the instantaneous powers calculation block to determine the real and imaginary powers, *p* and *q*, respectively. Low pass filters (LPF) are used to separate the oscillating real and imaginary powers $\tilde{p}$ and $\tilde{q}$ from *p* and *q*, respectively. If the active filter controller compensates only the oscillating powers, the source current should be purely sinusoidal since the active filter should provide the harmonic currents to the load. The αβ0 current calculation block uses $\tilde{p}$ and $\tilde{q}$ along with $v'_{(\alpha\beta0)}$ to calculate the compensating harmonic currents $i^*_{h(\alpha\beta0)}$. The inverse Clark transformation is used to calculate the compensation currents in the *abc*-axes $i^*_{h(abc)}$. Fig. 3 shows the block diagram of C1.

In C2, as in C1, a DSOGI-FLL is used to determinate the positive-sequence fundamental component $v'_{(\alpha\beta0)}$ of $v_{pcc(\alpha\beta0)}$. The source current $i_{S(abc)}$ and $v'_{(\alpha\beta0)}$ are used in the instantaneous powers calculation block to calculate *p* and *q*. LPFs are used to extract $\tilde{p}$ and $\tilde{q}$ from *p* and *q*. PI controllers are used to dynamically determine the real and imaginary power references, p^*_h and q^*_h, respectively. In C2, the PI controller proportional and integral gains are K_{pPQ} and K_{iPQ}, respectively. Unlike the strategy presented in [10], the harmonic detection strategy used in C2 is not selective and all harmonics besides the fundamental component are mitigated. The αβ0 current calculation block determines the compensating harmonic currents $i^*_{h(\alpha\beta0)}$ in αβ0-axes and the inverse Clarke transformation is used to calculate the compensation currents in the *abc*-axes $i^*_{h(abc)}$. Fig. 4 shows the block diagram of C2.

In C3, the positive-sequence fundamental components extracted from $v_{pcc(\alpha\beta0)}$ using the DSOGI-FLL are used as auxiliary currents $i'_{(\alpha\beta0)}$. Instantaneous powers *p* and *q* are calculated using $v_{pcc(\alpha\beta0)}$ and $i'_{(\alpha\beta0)}$ and its oscillating powers $\tilde{p}$ and $\tilde{q}$ are extracted from *p* and *q* using LPF. The αβ0 current calculation uses $\tilde{p}$ and $\tilde{q}$ along with $i'_{(\alpha\beta0)}$ to determinate the harmonic voltage $v_{h(\alpha\beta0)}$. Those harmonic voltages do not have a positive-sequence voltage component. The inverse Clark transformation is used to calculate the harmonic voltages in the *abc*-axes $v_{h(abc)}$ and the compensating harmonic current reference is given by (10).

$$i^*_{h(abc)} = K_v v_{h(abc)} \tag{10}$$

where K_v is the active filter control gain. Fig. 5 shows the block diagram of C3.

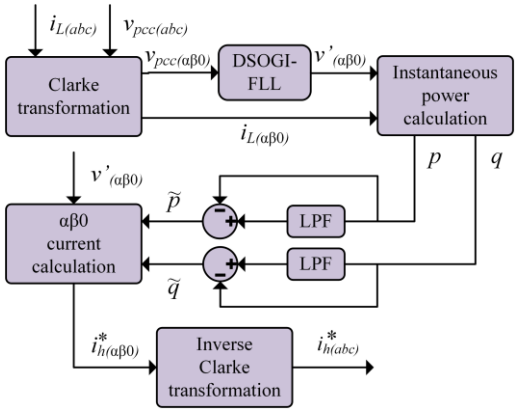

Fig. 3. Current harmonic detection block diagram for C1

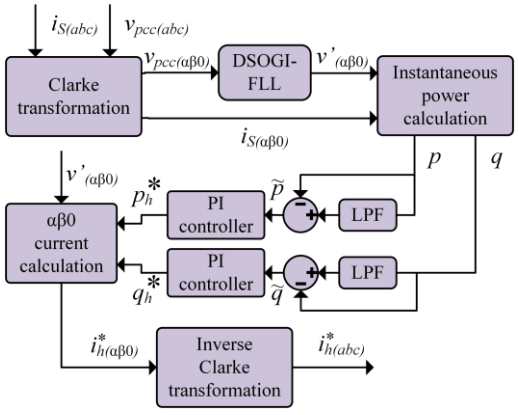

Fig. 4. Current harmonic detection block diagram for C2

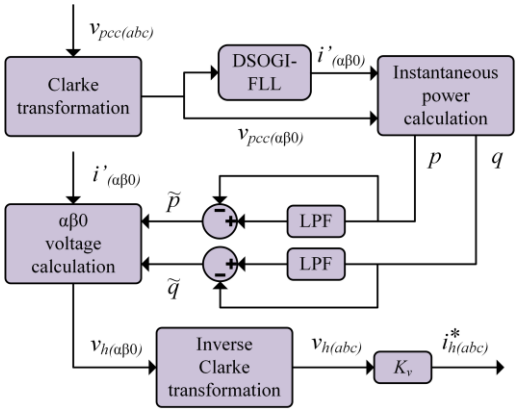

Fig. 5. Current harmonic detection block diagram for C3

In C1, the controller mitigates the harmonic currents of a feeder bus from the voltage and current measurements of a specific nonlinear load. In a reverse power flow scenario, the feeder bus current is measured instead of the load current. Thus, this controller would try to wrongly supply the harmonic currents to the feeder so that the load harmonic

current should be mitigated. In C2, the controller reduces the harmonic current of a feeder bus by measuring the voltage and current of the bus itself. Again, in a reverse power flow scenario, if this controller tries to compensate for a load bus current, it would try to reduce the load harmonic content. Thus, in C1 and C2, it is necessary to know the power flow on the bus for these strategies work properly. Although C3 does not measure currents to calculate the reference harmonic current and therefore is immune to variations in power flow, this controller cannot satisfactorily dampen the power system generators and substations voltage harmonics.

IV. Real-Time Simulation Results

To compare the three strategies presented in the paper, the presented algorithms were embedded in a real-time simulation test-bench using a Software-in-the-Loop (SIL) environment. A Typhoon Hardware-in-the-Loop HIL402 module is responsible for the real-time simulation of the power stage and the control system. The power stage for the real-time simulation was created using the Schematic Editor available in Typhoon HIL Control Center and the proposed VSG and harmonic detection controllers were implemented in C language. The supervision and system control are done through the Supervisory Control and Data Acquisition (SCADA) platform also available in Typhoon HIL Control Center. An oscilloscope was used to obtain the curves shown in this section and it was connected to the HIL402 through a breakout board. Fig. 6 presents the test-bench block diagram used in this work.

Fig. 6. Test-bench based on HIL402 module

The presented control strategies were simulated in two scenarios. In scenario 1 (S1), the infinite bus voltage has no voltage harmonics. In scenario 2 (S2), the voltage source has a 0.05 pu fifth harmonic. The harmonic voltage inserted in the voltage source represents the harmonic distortion present in a distribution system due to the circulation of harmonic currents in the feeders. S2 is necessary to evaluate the performance of all controllers under voltage harmonics profiles. Fig. 7 shows the proposed power system overview. The distribution system consists of a voltage source and a distribution feeder and its parameters are shown in Table I. The load consists of a set of linear and nonlinear loads and its parameters in both scenarios are shown in Table II. The renewable energy source is emulated by a DC voltage source (V_{DC}) and is connected to the grid through an inverter. The two-level, three-phase three-wire inverter is connected to the system through an LCL filter [21] and its parameters are shown in Table III. The inverter switches are IGBTs with anti-parallel diodes connected across. The inverter is operating with a switching frequency of 10 kHz. Controllers gains for each control strategy are shown in Table IV.

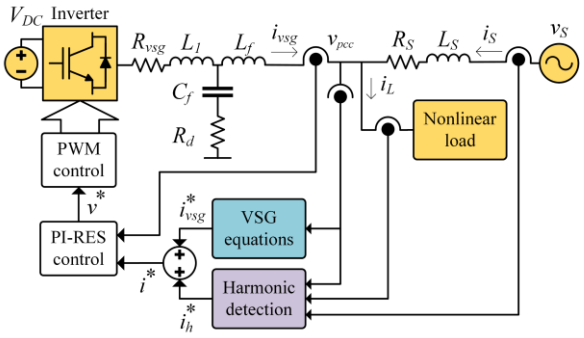

Fig. 7. Proposed power system overview

TABLE I
DISTRIBUTION SYSTEM AND VSG PARAMETERS

Parameters	Values
Source line voltage	220 V
Source resistance (R_s)	0.1 Ω
Source inductance (L_s)	0.6 mH
Link DC voltage (V_{DC})	500 V
VSG resistance (R_{vsg})	0.05 Ω
VSG inductance ($L_{vsg} = L_1+L_f$)	0.1613 mH
Virtual moment of inertia (J)	200 kg.m²
Damping factor (k_d)	0.3
Droop coefficient (D_p)	20

TABLE II
LOAD ACTIVE AND REACTIVE POWERS AND THD

Parameters	Load scenarios	
	S1	S2
Active power (kW)	18.60	18.68
Reactive power (kVAR)	5.26	5.28
I_{La} - THD (%)	12.68	11.63
I_{Lb} - THD (%)	11.45	9.28
I_{Lc} - THD (%)	11.52	8.07

TABLE III
LCL FILTER SPECIFICATION AND PARAMETERS

Parameters	Values
Switching frequency (f_s)	10 kHz
Nominal frequency (f_n)	60 Hz
Converter nominal power (P_n)	50 kW
Nominal line voltage (E)	220 V
Inductance (L_1)	0.1397 mH
Inductance (L_f)	0.0216 mH
Capacitance (C_f)	137.01 µF
Resistance (R_d)	0.75 Ω

The current controller is a proportional integral-resonant (PI-RES) controller [22] and its proportional, integral, and resonant gains are K_p, K_i, and K_r, respectively. The resonant controllers are tuned in the 6th and 12th harmonics. The gains used in each control strategy are shown in Table IV.

TABLE IV
CURRENT CONTROLLER GAINS

Parameters	Control strategy – S1 / S2		
	C1	C2	C3
Proportional gain (K_p)	2	0.5	0.25
Integral gain (K_i)	250	250	50
Resonant gain (K_r)	250	250	250
C2 proportional gain (K_{pPQ})	-	4	-
C2 integral gain (K_{iPQ})	-	50	-
C3 voltage gain (K_v)	-	-	3.5

Fig. 8 shows the source current in S1 before the inverter connection to the system. Source current harmonic contents are shown in Table V. CH1, CH2, and CH3 are the source current in the *a*, *b* and, *c* phases, respectively.

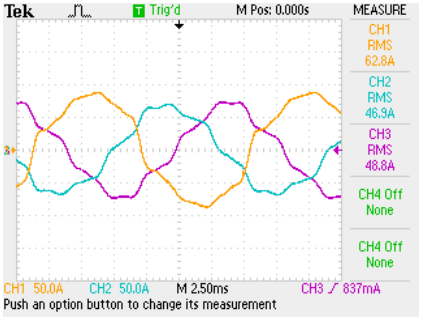

Fig. 8. Source current in S1 before compensation

The VSG controller calculates positive-sequence current components at the fundamental frequency according to the parameters shown in Table I while the harmonic detection controllers determine the compensation harmonic current. The compensated source currents for C1, C2, and C3 are shown in Fig. 9 and the source currents and the voltages at the PCC harmonic content for phases *abc* are shown in Tables V and VI, respectively.

In S1, C1, C2, and C3 were able to mitigate the harmonic currents from I_s as shown in Table V. In C1, source currents THD were reduced 78.9%, 77.5%, and 81.7% for phases *abc*, respectively. In C2, source currents THD were reduced 78.9%, 84.6%, and 71.9% for phases *abc*, respectively. In C3, source currents THD were reduced 66.9%, 76.1%, and 71.2% for phases *abc*, respectively.

Also, C1, C2, and C3 were able to mitigate the harmonic voltages from V_{pcc} as shown in Table VI. In C1, PCC voltages THD were reduced 75.8%, 66.2%, and 68.7% for phases *abc*, respectively. In C2, PCC voltages THD were reduced 72.5%, 65.9%, and 44.3% for phases *abc*, respectively. In C3, PCC voltages THD were reduced 71.4%, 73.2%, and 72.4% for phases *abc*, respectively. The reference voltage was set to 179.6 V and the VSG controller regulated it, as shown in Table VI.

While C1 and C2 were able to compensate the unbalanced currents from I_s, C3 does not compensate the unbalanced currents, since its goal is to damp the grid harmonic voltage.

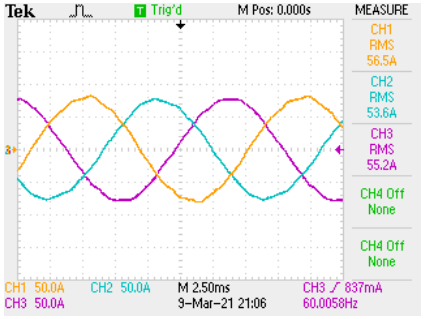

(a)

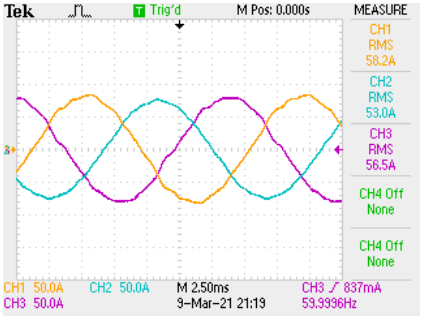

(b)

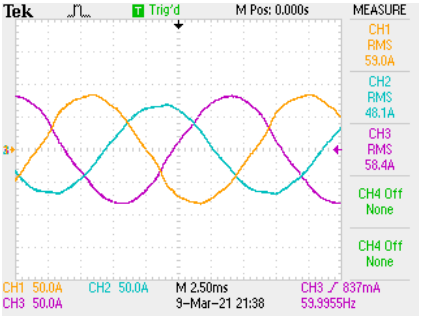

(c)

Fig. 9 - Compensated current using (a) C1, (b) C2, and (c) C3 in S1

TABLE V
SOURCE CURRENT HARMONIC CONTENT IN S1 BEFORE AND AFTER THE COMPENSATION

h	Before compensation			C1			C2			C3		
	A	b	c	a	b	c	a	b	c	a	b	c
1 (A)	87.3	66.74	66.87	79.13	76.20	78.20	81.09	75.03	78.06	82.78	68.52	82.54
3 (A)	5.99	3.02	2.98	0.64	1.03	0.74	0.63	0.23	0.83	2.41	0.63	2.05
5 (A)	5.98	4.49	4.38	0.69	0.93	0.50	1.16	0.31	0.99	1.68	0.40	1.51
7 (A)	5.98	4.72	4.72	0.73	0.52	0.49	1.11	0.78	1.09	2.03	1.08	1.09
9 (A)	1.94	1.06	0.95	0.23	0.96	0.62	0.15	0.64	0.75	0.42	0.07	0.32
11 (A)	2.96	2.23	2.07	1.27	0.68	0.84	1.32	0.46	1.29	0.69	0.13	0.39
13 (A)	1.76	1.52	1.47	0.34	0.61	0.56	0.34	0.72	0.86	0.48	0.26	0.49
THD (%)	12.68	11.45	11.52	2.68	2.58	2.11	2.67	1.76	3.24	4.20	2.74	3.32

TABLE VI
THE VOLTAGE AT THE PCC HARMONIC CONTENT IN S1 BEFORE AND AFTER THE COMPENSATION

h	Before compensation			C1			C2			C3		
	a	b	c	a	b	c	a	b	c	a	b	c
1 (V)	164.11	166.12	170.63	179.47	180.00	180.48	179.2	179.83	180.80	177.85	179.98	182.12
3 (V)	4.44	1.16	3.28	0.92	1.61	0.96	0.10	0.93	1.05	1.10	0.81	1.66
5 (V)	7.05	4.74	5.90	0.96	1.78	1.35	1.10	0.84	2.02	1.89	1.39	2.52
7 (V)	9.28	6.57	6.64	0.81	1.92	1.17	1.20	0.82	1.93	2.58	1.37	1.37
9 (V)	4.02	1.69	2.39	0.67	1.53	0.87	0.63	1.13	1.81	0.43	0.97	1.20
11 (V)	6.40	4.66	5.30	3.03	0.50	2.75	2.92	1.29	4.38	1.24	1.00	1.48
13 (V)	4.46	2.74	2.68	0.63	0.91	0.90	1.20	1.26	2.72	1.04	0.81	1.16
THD (%)	9.31	6.37	6.30	2.25	2.15	1.97	2.56	2.17	3.51	2.66	1.71	1.74

Fig. 10 shows the source current in S2 before the connection of the inverter to the system, and its harmonic content is shown in Table VII.

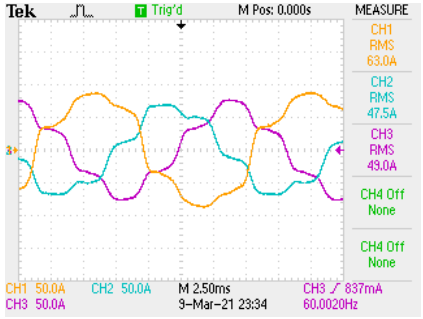

Fig. 10. Source current in S2 before compensation

The compensated source currents for C1, C2, C3 are shown in Fig. 11 and the source currents and the voltages at the PCC harmonic content for phases *abc* are shown in Tables VII and VIII, respectively. VSG and harmonic detection parameters are the same used in S1.

Despite the harmonic voltage in the voltage source in S2, C1 and C2 were able to mitigate the harmonic currents from I_s as shown in Table VII. In C1, source currents THD were reduced 79.6%, 83.8%, and 86.1% for phases *abc*, respectively. In C2, source currents THD were reduced 80.6%, 89.2%, and 81.1% for phases *abc*, respectively. The performance of C3 harmonic current mitigation is not as good as the performances for C1 and C2. Since C3 aims to damp the harmonic voltages from V_{pcc}, this strategy could not properly mitigate the fifth harmonic current generated by the fifth voltage harmonic of the system voltage source. In C3, source currents THD were reduced 34.2%, 24.5% and 33.6%, for phases *abc*, respectively.

However, C3 was able to mitigate the harmonic voltages from V_{pcc} while C1 and C2 could not properly mitigate the fifth harmonic voltage, as shown in Table VIII. While both C1 and C2 aim to compensate harmonic currents from the source currents, these strategies could not mitigate the fifth harmonic voltages caused by the voltage source as they are not designed for it.

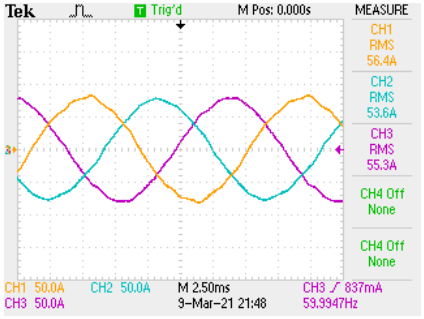

(a)

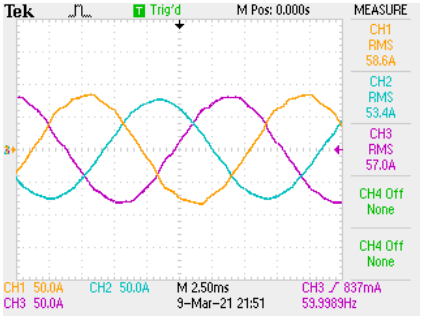

(b)

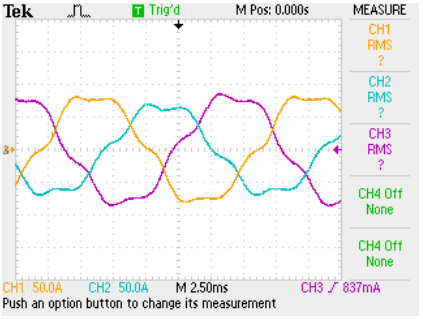

(c)

Fig. 11 - Compensated current using (a) C1, (b) C2, and (c) C3 in S2

TABLE VII
SOURCE CURRENT HARMONIC CONTENT IN S2 BEFORE AND AFTER THE COMPENSATION

h	Before compensation			C1			C2			C3		
	a	b	c	a	b	c	a	b	c	a	b	c
1 (A)	87.22	66.49	67.69	79.18	76.28	78.4	82.44	75.62	79.98	82.29	68.94	84.03
3 (A)	6.63	2.60	4.04	0.83	1.00	0.68	0.93	0.24	1.05	2.46	0.71	1.65
5 (A)	10.50	8.81	9.54	1.51	1.25	0.73	1.08	0.41	0.88	8.42	7.97	9.03
7 (A)	6.43	5.22	3.99	0.82	0.51	0.46	1.64	0.86	1.18	1.83	0.97	1.12
9 (A)	1.83	1.27	0.69	0.27	0.93	0.53	0.31	0.84	0.65	0.38	0.12	0.36
11 (A)	2.25	1.86	1.83	1.21	0.57	0.79	1.59	0.41	1.24	0.42	0.18	0.43
13 (A)	1.50	1.42	0.61	0.46	0.63	0.63	0.26	0.43	0.60	0.45	0.23	0.41
THD (%)	16.58	16.05	16.55	3.39	2.60	2.30	3.21	1.74	3.12	10.91	12.11	10.93

TABLE VIII
THE VOLTAGE AT THE PCC HARMONIC CONTENT IN S2 BEFORE AND AFTER THE COMPENSATION

h	Before compensation			C1			C2			C3		
	a	b	c	a	b	c	a	b	c	a	b	c
1 (V)	164.15	164.83	168.53	179.49	179.97	180.44	179.14	179.74	179.14	177.69	180.26	180.09
3 (V)	4.06	2.71	1.29	1.03	1.54	0.83	0.20	0.88	0.97	1.21	0.53	0.64
5 (V)	11.84	12.08	9.87	10.47	8.76	9.03	9.40	8.46	9.82	3.23	2.34	2.24
7 (V)	9.86	9.05	7.08	0.98	1.88	1.05	2.13	0.42	0.28	2.60	1.35	1.76
9 (V)	3.99	2.96	1.55	0.76	1.47	0.75	0.09	1.71	0.53	0.46	0.66	0.97
11 (V)	6.01	3.92	3.37	3.10	0.38	2.69	3.83	0.26	2.12	0.74	0.77	0.46
13 (V)	5.27	4.66	3.92	1.06	1.23	1.19	1.23	0.35	1.92	1.08	0.61	0.89
THD (%)	11.63	9.28	8.07	6.25	5.48	5.72	5.87	5.15	5.64	3.09	2.35	2.13

In C1, PCC voltages THD were reduced 46.3%, 40.9%, and 29.1% for phases *abc*, respectively. In C2, PCC voltages THD were reduced 49.5%, 44.5%, and 30.1% for phases *abc*, respectively. In C3, PCC voltages THD were reduced 73.4%, 74.7%, and 73.6% for phases *abc*, respectively. The reference voltage was set to 179.6 V and the VSG controller regulated it, as shown in Table VIII.

To evaluate that the combination of VSG and active filter controls can reduce the frequency variation at the PCC during system loads (P_{Load} and Q_{Load}) and VSG P_{ref} changes, the proposed controls were compared with a combination of a constant active and reactive power control (PQ control) based on *pq* Theory and the active filter controls presented in Section III. In the proposed simulation, at t = 0.2 s, the load is increased from P_{Load} = 18.95 kW and Q_{Load} = 6.22 kVAR to P_{Load} = 23.78 kW and Q_{Load} = 10.29 kVAR. At t = 1.2 s, VSG active power reference is changed from P_{ref} = 20 kW to P_{ref} = 30 kW. The step change in P_{ref} is done to show the VSG control inertial behavior. A null reactive reference power (Q_{ref} = 0) was chosen during the simulation since the goal is to compare the VSG and PQ active power controls in response to frequency variations. Thus, the contribution of frequency stability is only and exclusively provided for active power control and it is possible to highlight the contribution of the synthetic inertia provided by the VSG active power control when compared to the PQ active power control in response to frequency variations.

Error! Reference source not found. shows inverter active and reactive powers (P_{inv} and Q_{inv}, respectively), frequency (*Freq*), angular velocity deviation of the voltage synthesized by the inverter (*dw*), and PCC voltage for the combinations of PQ and VSG controls with the active filter control strategy C1 (C1PQ and C1VSG, respectively), the combinations of PQ and VSG controls with the active filter control strategy C2 (C2PQ and C2VSG, respectively), and the combinations of PQ and VSG controls with the active filter control strategy C3 (C3PQ and C3VSG, respectively). Table IX shows the frequency variation of active filter and PQ (Δf_{PQ}) and active filter and VSG (Δf_{VSG}) controllers after the load change in t = 0.2 s and the inverter active power reference (P_{ref}) change in t = 1.2 s. The percentage reduction (PR) obtained with the VSG control is also shown in Table IX.

As shown in Fig. 12 and Table IX, the VSG control can reduce the frequency variation during system load and VSG P_{ref} changes. The VSG control provides synthetic inertia to the voltage synthesized by the inverter, as shown in the angular velocity deviation curves. The VSG control slows down the active power response and reduces the angular velocity deviation during disturbances. Consequently, it can mitigate the voltage frequency variation at the PCC. Voltage at the PCC is not controlled since Q_{ref} = 0 during the simulation. Due to time and phase delays, a feedback control loop between the detected harmonic voltage and the compensating harmonic current can contribute to instability or can deteriorate the harmonic damping performance of the active filter based on C3 [5].

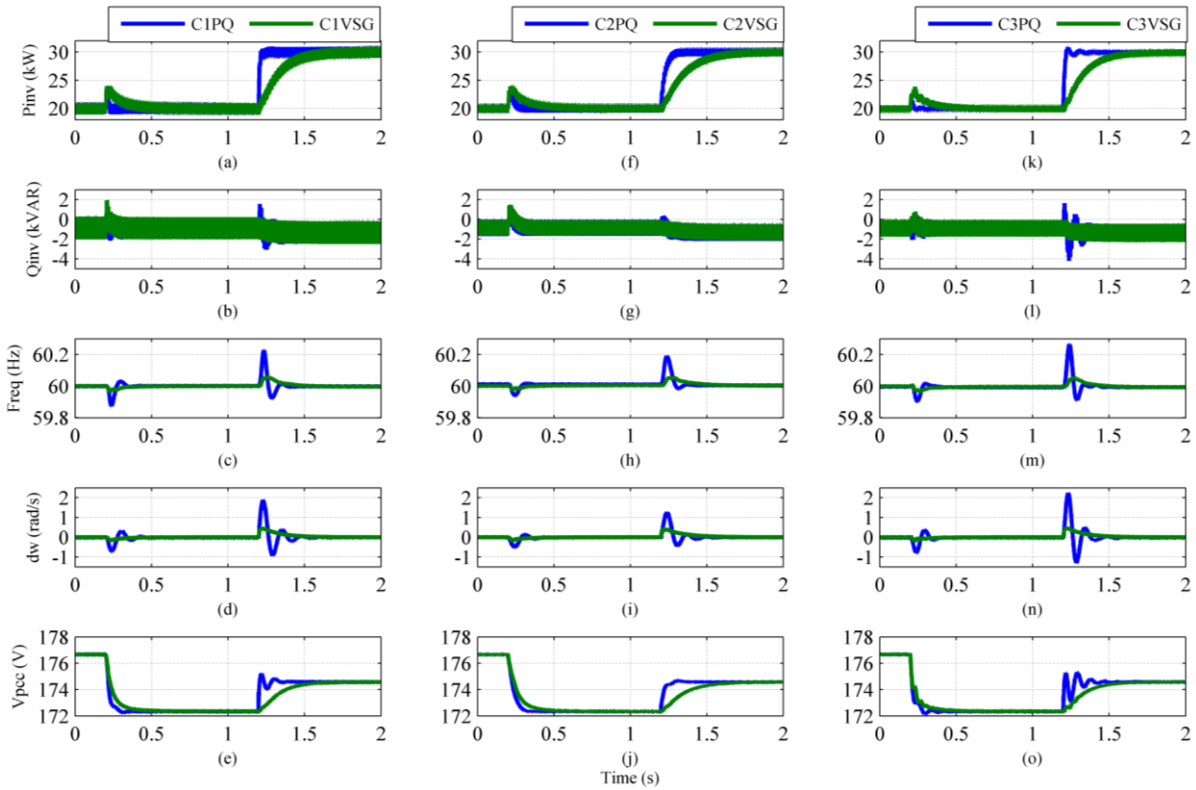

Fig. 12 - (a) VSG active and (b) reactive powers, (c) frequency, (d) angular velocity deviation, and (e) PCC voltage for C1PQ and C1VSG controls; (f) VSG active and (g) reactive powers, (h) frequency, (i) angular velocity deviation, and (j) PCC voltage for C2PQ and C2VSG controls; and (k) VSG active and (l) reactive powers, (m) frequency, (n) angular velocity deviation, and (o) PCC voltage for C3PQ and C3VSG controls

TABLE IX
FREQUENCY VARIATION OF ACTIVE FILTER AND PQ CONTROLS AND ACTIVE FILTER AND VSG CONTROLS DURING LOAD AND PREF CHANGES

AF control	Load change - t = 0.2 s			P_{ref} change - t = 1.2 s		
	Δf_{PQ} (Hz)	Δf_{VSG} (Hz)	PR (%)	Δf_{PQ} (Hz)	Δf_{VSG} (Hz)	PR (%)
C1	0.15	0.05	66.7	0.30	0.07	76.7
C2	0.08	0.03	62.5	0.20	0.06	70.0
C3	0.11	0.05	54.5	0.35	0.06	82.9

V. CONCLUSIONS

This paper presented three control strategies that combine VSG and active filter capabilities. Fig. 8 to Fig. 11 and Tables V to VIII show that the proposed controllers can mitigate the source harmonic currents and voltages while regulating the voltage at the PCC in both scenarios.

While all presented active filter control strategies can work properly in S1, they have some limitations if the source voltage has harmonics. In S2, C1 and C2 can mitigate the source harmonic currents, but they can not mitigate the fifth harmonic voltage at the PCC, since these strategies aim to compensate harmonic currents. In S2, C3 can damp the harmonic voltages at the PCC, but it can not mitigate the fifth harmonic source current, since this strategy aims to damp the harmonic voltages at the PCC.

The control strategy C3 only measures voltages to determine the harmonic current reference. This strategy would not be affected by the unpredictable power flow caused by the addition of new DGs and grid reconfigurations which could change the power flow. In turn, this would not compromise the active filter control strategy, since it does not measure any currents to calculate the active filter current references. Thus, C3 is more suitable for electric power utilities, since it does not seek to solve problems from specific customers. However, C1 and C2 only work properly in a unidirectional power flow distribution system. These control strategies would not work well in a grid with DG with bidirectional power flow and they are more suitable for end-users or individual customers.

In both scenarios, the VSG controller reference peak voltage V_0 was 179.61 V and the voltage at the PCC after the inverter connection to the system was properly regulated by the VSG controller as seen in Tables VI and VIII. Furthermore, C1 and C2 were able to compensate for the unbalanced feeder currents in both scenarios as seen in Fig. 9 (a) and (b) and Fig. 11 (a) and (b), respectively.

The combination of the active filter controllers and the VSG controller was compared to a combination of the active filter controller and a PQ controller based on *pq* Theory. As shown in Fig. 12 and Table IX, the VSG controller can reduce the frequency variations during disturbances as expected, improving the system stability.

VI. REFERENCES

[1] G. Pepermans, J. Driesen, D. Haeseldonckx, R. Belmans and W. D'haeseleer, "Distributed generation: definition, benefits and issues," *Energy Policy*, vol. 33, issue 6, pp. 787-798, 2005.

[2] J. Driesen and K. Visscher, "Virtual synchronous generators," in *Proc. 2008 IEEE Power and Energy Society General Meeting - Conversion and Delivery of Electrical Energy in the 21st Century*, Pittsburgh, PA, 2008, pp. 1-3.

[3] P. Kundur, J. Paserba, V. Ajjarapu, G. Andersson, A. Bose, C. Canizares, N. Hatziargyriou, D. Hill, A. Stankovic, C. Taylor, T. Van Cutsem and V. Vittal, "Definition and classification of power system stability IEEE/CIGRE joint task force on stability terms and definitions," *IEEE Transactions on Power Systems*, vol. 19, issue 3, pp. 1387-1401, Aug. 2004.

[4] K. M. Cheema, "A comprehensive review of virtual synchronous generator," *International Journal of Electrical Power & Energy Systems*, vol. 120, pp. 1-10, Sep. 2020.

[5] H. Akagi, E. H. Watanabe and M. Aredes, *Instantaneous power theory and applications to power conditioning*, IEEE Press Series on Power Engineering. New Jersey: John Wiley & Sons, 2007.

[6] L. Morán; J. Dixon, "Active Filters," in *Power Electronics Handbook*, 2nd ed., M. H. Rashid, Burlington: Academic, 2006. p. 1067-1102.

[7] W. N. Sepulchro, L. F. Encarnação, M. Brunoro, "Harmonic State and Power Flow Estimation in Distribution Systems Using Evolutionary Strategy." *Journal of Control, Automation and Electrical Systems*, vol. 25, pp. 358-367, 2014.

[8] *IEEE Recommended Practice and Requirements for Harmonic Control in Electric Power Systems*, IEEE Std 519-2014 (Revision of IEEE Std 519-1992), Jun. 2014.

[9] Z. Qu, H. Yang, Y. Cai and H. Wang, "Application of virtual synchronous generator technology in three-phase four-leg inverter," in *Proc. 2017 20th International Conference on Electrical Machines and Systems* (ICEMS), Sydney, NSW, 2017, pp. 1-6.

[10] T. S. Amorim, D. Carletti, L. F. Encarnação, "Enhanced Virtual Synchronous Generator with Harmonic Current Filtering Capability," in *Proc. IECON 2019 - 45th Annual Conference of the IEEE Industrial Electronics Society*, Lisbon, Portugal, pp 1732-1737.

[11] T. S. Amorim, D. Carletti, L. F. Encarnação, "Virtual Synchronous Generator with Harmonic Current Filtering Capability Based on Voltage Detection," in *Proc. 2019 IEEE PES Innovative Smart Grid Technologies Europe* (ISGT-Europe), Bucharest, Romania, pp. 1-5.

[12] Mai Diab, M. El-Habrouk, T. H. Abdelhamid and S. Deghedie, "Survey of Active Power Filters Configurations," in *Proc. 2018 IEEE International Conference on System, Computation, Automation and Networking* (ICSCA), Pondicherry, India, pp. 1-14.

[13] M. Torres, J. Espinoza, L. Morán, J. Rohten and P. Melín, "Integration of a large-scale photovoltaic plant using a multilevel converter topology and virtual synchronous generator control," in *Proc 2014 IEEE 23rd International Symposium on Industrial Electronics* (ISIE), Istanbul, Turkey, pp. 2620-2624.

[14] D. Panda, B.S. Raipurohit, A. Monti, "Synthetic Inertia for Frequency Regulation of Electric Grid using Modular-Multilevel Converter," in Proc. 2019 IEEE Industry Applications Society Annual Meeting, Baltimore, USA, pp. 1-8.

[15] E. Can, "Novel high multilevel inverters investigated on simulation." *Electrical Engineering*, vol. 99, pp. 633-638, 2017.

[16] L. F. Encarnação, D. Carletti, S. A. Souza, O. Barros Jr., D. C. Broedel and P. T. Rodrigues, "11 - Virtual Inertia for Power Converter Control," in *Advances in Renewable Energies and Power Technologies*, I. Yahyaoui, Elsevier, 2018, pp. 377-411.

[17] H. Bevrani, T. Ise and Y. Miura, "Virtual synchronous generators: A survey and new perspectives," *International Journal of Electrical Power & Energy Systems*, vol. 54, 2014, pp. 244-254.

[18] S. D'Arco and J. A. Suul, "Virtual synchronous machines – Classification of Implementations and Analysis of Equivalence to Droop Controllers for Microgrids," in *Proc. 2013 IEEE Grenoble Conference*, Grenoble, France, pp. 1-7.

[19] Y. Chen, R. Hesse, D. Turschner and H. P. Beck, "Improving the grid power quality using virtual synchronous machines," in *Proc. 2011 International Conference on Power Engineering, Energy and Electrical Drives*, Malaga, Spain, pp. 1-6.

[20] P. Rodriguez, A. Luna, M. Ciobotaru, R. Teodorescu and F. Blaabjerg, "Advanced Grid Synchronization System for Power Converters under Unbalanced and Distorted Operating Conditions," in *Proc. IECON 2006 - 32nd Annual Conference on IEEE Industrial Electronics*, Paris, France, pp. 5173-5178

[21] M. Liserre, F. Blaabjerg and S. Hansen, "Design and control of an LCL-filter-based three-phase active rectifier," *IEEE Transactions on Industry Applications*, vol. 41, no. 5, pp. 1281-1291, Sept.-Oct. 2005.

[22] M. Liserre, R. Teodorescu and F. Blaabjerg, "Multiple harmonics control for three-phase grid converter systems with the use of PI-RES current controller in a rotating frame," *IEEE Transactions on Power Electronics*, vol. 21, no. 3, pp. 836-841, May 2006.